The Component of "Ruthenium Red" Responsible for Inhibition of Mitochondrial Calcium Ion Transport. Spectra, Electrochemistry, and Aquation Kinetics. Crystal Structure of μ-O-$[(HCO_2)(NH_3)_4Ru]_2Cl_3$

Jeffrey Emerson,† M. J. Clarke,*,† Wen-Long Ying,‡ and D. Rao Sanadi‡

Contribution from the Department of Chemistry, Boston College, Chestnut Hill, Massachusetts 02167, and Department of Cell Physiology, Boston Biomedical Research Institute, 20 Staniford Street, Boston, Massachusetts 02114

Received August 17, 1993®

Abstract: The cytological stain, ruthenium red, effectively inhibits mitochondrial Ca^{2+}_{aq} uptake; however, the majority of this activity has been attributed to an impurity. This component has now been isolated and a derivative, μ-O-$[(HCO_2)(NH_3)_4Ru]_2Cl_3$, characterized by X-ray diffraction, spectroscopy, and electrochemistry. The compound crystallizes in the orthorhombic space group *Pnn2* (No. 34), with unit cell constants of a = 8.588 (1), b = 13.335 (2), c = 7.602 (2) Å, Z = 2, and R = 0.024. The bridging Ru–O bond is quite short (1.8240(6) Å), while the $Ru–O_{formate}$ bond length (2.033(3) Å) is typical for a Ru–O single bond. The equatorial ammine–ruthenium bond lengths average 2.11(2) Å. The placement of the μ-O on a crystallographic two-fold axis dictates that the two metal centers are identical. The crystallographic equivalence together with electrochemical evidence ($E°$ = 1.17 and 0.05 V) indicates strong electronic coupling between the mixed-valent ruthenium centers. The apical formates are easily replaced by chlorides in HCl. Aquation rates of both the formato and chloro complexes are pH dependent. For the formato complex k_{obs} is given by $k_{obs} = (k_1[H^+]^2 + k_2[H^+]K_{a1} + k_3K_{a1}K_{a2})/([H^+]^2 + [H^+]K_a + K_{a1}K_{a2})$, where k_1 = (7.8 ± 0.1) × 10^{-3} s^{-1}, k_2 = (1.2 ± 0.1) × 10^{-4} s^{-1}, k_3 = ~4 × 10^{-4} s^{-1}, pK_{a1} = 2.45 ± 0.07, and pK_{a2} = ~9. The active species in solution appears to be the oxo-bridged ion, $[X(NH_3)_4Ru–O–Ru(NH_3)_4X]^{3+}$, where X = Cl^- or OH^-. The hydroxo-capped complex decomposes above pH 7. Theoretical calculations show these ions to be highly deformable, which may partially explain their ability to inhibit Ca^{2+} binding to a number of different sites.

The mixed-valent complex, ruthenium red, has reached its centennial of use as a cytological stain[1] and has recently been widely investigated as a drug interfering with calcium utilization.[2,3] Originally employed to visualize pectins in plant cell walls by light microscopy, it is a generic stain for polyanions with high charge density, such as acidic mucopolysaccharides and DNA,[4] and has been used for the past three decades as a selective stain for mitochondria and muscle fibrils in both visible and electron microscopy.[5] Its chemical and physiological properties have been previously summarized.[6]

Aside from its extensive histochemical use, ruthenium red is useful as a gel stain for a variety of Ca^{2+}-binding proteins with different types of Ca^{2+}-binding sites.[7] It inhibits Ca^{2+} binding to calmodulin[3] and specifically inhibits uptake of Ca^{2+} by affecting both the Ca^{2+}-pump and -release mechanism.[8] Nanomolar levels of ruthenium red strongly inhibit respiration-driven Ca^{2+}_{aq} uptake in mitochondria.[9,10] Ruthenium red also blocks Ca^{2+} transport in other systems including the Ca^{2+} release channels of the sarcoplasmic reticulum,[11,12] voltage-dependent Ca^{2+} channels in cisplatin-sensitive and -resistant leukemia cells,[13] as well as Ca^{2+} sequestration in the endoplasmic reticulum.[14] Since micromolar concentrations of ruthenium red can reduce calcium accumulation by isolated nerve endings as well as mitochondria, it interferes with nerve transmission by reducing neurotransmitter release[15] and may also exert an effect by binding to sialic acid residues,[16] Higher concentrations induce neurotoxicity and paralysis.[6,17] Its effect on calcium metabolism has also been linked to inhibition of tumor growth.[18]

The affinity of ruthenium red for mucopolysaccharides has been used to visualize tumors that often produce a protective coating consisting largely of hyaluronic acid.[19] In this technique, a γ-emitting isotope, ^{103}Ru or ^{97}Ru, is used to synthesize ruthenium red and imaging is effected by monitoring the radiation localized in the tumor.[20,21]

While ruthenium red is well characterized and has the structure[22] $[(NH_3)_5Ru^{III}–O–(NH_3)_4Ru^{IV}–O–Ru^{III}(NH_3)_5]^{6+}$, its commercial preparations are often less than 20% pure.[23] Major

† Boston College, Clarke@Hermes.BC.edu.
‡ Boston Biomedical.
® Abstract published in *Advance ACS Abstracts*, November 15, 1993.

(1) Mangin, L. *C. R. Acad. Sci. (Paris)* **1893**, *116*, 653–656.
(2) Corbalan-Garcia, S.; Teruel, J. A.; Gomez-Fernandez, J. C. *Biochem. J.* **1992**, *287*, 767.
(3) Sasaki, T.; Naka, M.; Nakamura, F. *J. Biol. Chem.* **1992**, *267*, 21518.
(4) Murano, E.; Paoletti, S.; Cesaro, A. *Anal. Biochem.* **1990**, *187*, 120–124.
(5) Hirabayashi, Y.; Sakagami, T.; Yamada, K. *Acta Histochem. Cytochem.* **1990**, *23*, 165–175.
(6) Clarke, M. J. *Met. Ions Biol. Syst.* **1980**, *11*, 231–283.
(7) Charuk, J. H.; Pirraglia, C. A.; Reithmeier, R. A. *Anal. Biochem.* **1990**, *188*, 123–131.
(8) Meszaros, L.; Ikemoto, N. *Biophys. Biochem. Res. Commun.* **1985**, *127*, 836–842.
(9) Reed, K. C.; Bygrave, F. L. *Biochem. J.* **1974**, *140*, 143–155.
(10) Reed, K. C.; Bygrave, F. L. *FEBS Lett.* **1974**, *46*, 109–114.
(11) Antoniu, B.; Kim, D. H.; Morii, M.; Ikemoto, N. *Biochim. Biophys. Acta* **1985**, *816*, 9–17.
(12) Chiesi, M.; Schwaller, R.; Galviello, G. *Biochem. Biophys. Res. Commun.* **1988**, *154*, 1–8.
(13) Vassilev, P. M.; Kanazirska, M. P.; Charamella, L. J.; Dimitrov, N. V.; Tien, H. T. *Cancer Res.* **1987**, *47*, 519–522.
(14) Hurley, T. W. *Am. J. Physiol.* **1988**, *23*, 621–627.
(15) Taipale, H. T.; Kauppinen, R. A.; Komulainen, H. *Biochem. Pharm.* **1989**, *38*, 1109–1113.
(16) Wieraszko, A. *Brain Res.* **1986**, *378*, 120–127.
(17) Tapia, R. *Neurosci. Lett.* **1982**, *30*, 73–77.
(18) Anghileri, L. J.; Marchal, C.; Matrat, M.; Crone-Escanya, M. C. *Neoplasma* **1986**, *33*, 603–608.
(19) Oberc-Greenwood, M. A.; Muul, L. M.; Gately, M. K.; Kornblith, P. L.; Smith, B. W. *J. Neuro-Oncol.* **1986**, *3*, 387–396.
(20) Srivastava, S. C.; Mausner, L. F.; Clarke, M. J. In *Ruthenium and other Non-Platinum Metal Complexes in Cancer Chemotherapy*; Clarke, M. J., Ed.; Springer-Verlag: Heidleberg, Germany, 1989; Vol. 10, pp 111–150.
(21) Anghileri, L. H. *Strahlentherapie* **1975**, *149*, 173–175.
(22) Carrondo, M. A. A. F. d. C. T.; Griffith, W. P.; Hall, J. P.; Skapski, A. C. *Biochem. Biophys. Acta* **1980**, *627*, 332–334.
(23) Luft, J. H. *Anat. Rec.* **1971**, *171*, 347–368.

0002-7863/93/1515-11799$04.00/0

impurities absorbing at 355 nm, which are present even in samples purified by a standard selective precipitation technique,[2,3,23] produce a stronger inhibition of calcium ion uptake in mitochondria than chromatographically purified ruthenium red.[10] These components have recently been shown to be oxygen-bridged, dimeric species,[24] whose chemistry is described here along with the crystal structure of a closely related complex, μ-O-$[(HCO_2)(NH_3)_4Ru]_2Cl_3$, which is obtained by formate substitution. Consistent with earlier studies,[10,25] this dinuclear complex and its precursor species are strong inhibitors of Ca^{2+} for the receptor protein in the Ca^{2+} uniporter.[24] Aside from their biological activity, oxo-bridged ruthenium dinuclear species are of interest as redox catalysts for the important oxidations of water to oxygen, of chloride to chlorine, and of several organic substrates.[26-28]

Experimental Section

Synthesis. $RuCl_3 \cdot H_2O$ (250 mg) was dissolved in 1.5 mL of 6 M HCl, and 0.2 mL of absolute ethanol was added. In order to reduce any Ru^{IV} normally present in the commercial material to Ru^{III}, the ethanol solution was placed in a water bath at 90 °C for 1 h. This was followed by the addition of 0.2 mL of aqueous ammonia, which immediately produced a heavy, black, granular precipitate. The precipitate was collected by centrifugation, resuspended in 20 mL of 12 M NH_3, placed in a covered container, maintained at 90 °C for 20 min, and then held at 40 °C overnight. The portion of the precipitate that remained was removed by centrifugation, and the supernatant, which contained about 40% of the ruthenium dimer absorbing at 360 nm and 10% ruthenium red, was diluted with water (~1.1 L) and adjusted with 5 M formic acid (~45 mL) to be 0.2 M in ammonium formate (pH 5.5) and loaded onto a 1.5- × 10-cm Whatman CM-52 column previously equilibrated with 0.2 M ammonium formate. The column was eluted with a linear ammonium formate gradient from 0.2 to 0.4 M. Substantial amounts of a dark material generally remained at the top of the column. A yellowish fraction (λ_{max} = 360 nm) eluted with ~0.4 M ammonium formate and was lyophilized to remove the buffer. After the residue was dissolved in 5 mL of distilled water, 20 mL of absolute ethanol was slowly added with stirring to precipitate the desired material while leaving the $NH_4(O_2CH)$ in solution. The precipitate was similarly redissolved and precipitated twice more. The final precipitate (17 mg), which is presumably a formate salt, was dried at room temperature and stored in the refrigerator. The combined supernatants contained an additional ~4 mg of the dimeric product. Further purification could be effected by ion-exchange chromatography on BioRex 70 (400 mesh) resin eluted with 1.2 M $NH_4(O_2CH)$. Repurification of samples by this method often revealed small amounts of a darker, highly charged substance adhering to the top of the column.

The formate counter ion was exchanged for chloride by passing a solution through a CM-Sephadex or DEAE cellulose chloride column eluted with distilled water. The compound was then lyophilized to dryness. Crystals were obtained by dissolving 30 mg of the compound in 0.1 mL of water in a test tube and allowing ethanol to diffuse into the solvent by placing the test tube into a beaker containing 10 mL of ethanol and covering the assembly tightly with Parafilm. After 2 days, ~5 mg of irregular hexagonal red crystals were collected by decanting the supernatant from the test tube. Anal. Calcd. for $H_{26}C_2N_8O_5Ru_2Cl_3$: H, 4.76; C, 4.36; N, 20.34; Cl, 19.31; Ru, 36.70. Found: H, 5.10; C, 4.89; N, 20.16; Cl, 19.89; Ru, 36.5. $\mu_{eff} = 2.5 \pm 0.2\beta$ at 295 K. HPLC: $k' = 4.0$. ESR (77 °C, ethylene glycol/water): broad signal centered at $g = 2.06$.

The chloride-capped compound, μ-O-$[Cl_2(NH_3)_4Ru]_2Cl_3$, was prepared by dissolving 25 mg of μ-O-$[(HCO_2)(NH_3)_4Ru]_2Cl_3$ in 3 mL of water, loading it onto a Dowex 50W-X2 cation-exchange column (0.5 × 5 cm in a Pasteur pipet), and eluting it with a linear gradient of 1–4 M HCl. The desired complex eluted as a band in 3.5 M HCl, which was rotary evaporated to dryness. The residue was redissolved in a minimum of water and reprecipitated upon the addition of ethanol. Dark green crystals were obtained by ethanol diffusion into an aqueous solution of the complex. Anal. Calcd. for $H_{24}N_8ORu_2Cl_5 \cdot 0.5H_2O$: H, 4.66; N, 20.73; Cl, 32.79; Ru, 37.39. Found: H, 4.65; N, 20.89; Cl, 34.98; Ru, 37.02. $\mu_{eff} = 3.29 \pm 0.15\beta$ at 295 K. HPLC: $k' = 4.2$.

The diaqua compound, μ-O-$[(H_2O)_2(NH_3)_4Ru]_2(ClO_4)_5 \cdot 2H_2O$, was prepared by loading either the chloro or formato complexes onto a Sephadex SP-25 ion-exchange column that had been pretreated with 0.1 M $HClO_4$. The column was eluted with a gradient of 0.1–0.5 M $HClO_4$ in which the desired complex began to move as a green band in 0.2 M acid. After elution was complete, the band was rotary evaporated and redissolved in a minimum of water. The compound was precipitated as a gray powder from the acidic solution (pH ~2) by adding approximately 4 volumes of ethanol. Anal. Calcd. for $H_{28}N_8O_{23}Ru_2Cl_5$: H, 3.18; N, 12.62; Cl, 19.77; Ru, 22.77. Found: H, 3.28; N, 13.01; Cl, 19.91; Ru, 23.09.

Compound Characterization. Analyses for Ru were done by atomic absorption.[29] pK_a values were determined from spectrophotometric titrations. Magnetic susceptibility studies were performed on a Cahn Model 7500 Electrobalance at 23 °C and corrected for the diamagnetic contributions of the atoms.[30] UV–visible spectra were obtained on a Cary Model 2400. HPLC was performed on a 100- × 4.6-mm 3-μm C_{18} column monitored at 254 nm with a solvent (0.4 M ammonium propionate, pH 7.39) flow of 1.00 mL/min.

Electrochemical measurements were performed by cyclic or square-wave voltammetry in 0.1 M LiCl or $LiClO_4$ on a versatile electrochemical apparatus constructed in this laboratory. A carbon paste or platinum button working electrode, Ag/AgCl reference electrode, and platinum wire auxiliary electrode were used in all measurements. Reduction potentials were determined as the peak potential in square-wave voltammetric scans and by the average of the anodic and cathodic peak potentials from cyclic voltammetric scans. All potentials were internally referenced against the $[(NH_3)_6Ru]^{3+,2+}$ couple (57 mV vs NHE).

Crystallography. The structure of μ-O-$[(HCO_2)(NH_3)_4Ru]_2Cl_3$ was determined by mounting a single crystal on a glass fiber, which was placed in the beam of a Rigaku AFC5R diffractometer for data collection. On the basis of the systematic absences of $0kl$ with $k + l \neq 2n$ and $h0l$ with $h + l \neq 2n$, the space group was determined to be *Pnn2*. Crystallographic data are summarized in Table I, and atomic positions

Table I. Crystallographic Data for μ-O-$[(HCO_2)(NH_3)_4Ru]_2Cl_3$[a]

formula	$H_{26}C_2N_8O_5Cl_3Ru$
fw	550.78
space group, crystal system	*Pnn2* (No. 34), orthorhombic
cell constants	a = 8.588(1) Å b = 13.335(2) Å c = 7.602(2) Å
cell volume	870.6(3) Å^3
Z (fw/unit cell)	2
crystal dimensions (mm)	0.20 × 0.20 × 0.30
radiation source	Mo Kα λ = 0.71069 Å (graphite monochromated)
d_{calcd} (g/cm^3)	2.101
μ, rel. trans. factors	21.941 cm^{-1}, 0.81–1.0
$R = \frac{\sum(\lvert F_o\rvert - \lvert F_c\rvert)}{\sum\lvert F_o\rvert}$	0.024
$R_w = \left[\frac{\sum w(\lvert F_o\rvert - \lvert F_c\rvert)^2}{\sum w\lvert F_o\rvert^2}\right]^{1/2}$ [b]	0.033
goodness of fit = $\frac{\sum w(\lvert F_o\rvert - \lvert F_c\rvert)/\sigma}{N_{obs} - N_{parameters}}$ [c]	1.42

[a] T = 23(1) °C. Reflections with $I_0 > 3\sigma(I_0)$ were retained as observed and used in the solution and refinement of the structure. Three standard reflections were monitored with a limit of 0.2% variation. Function minimized $\sum w(\lvert F_o\rvert - \lvert F_c\rvert)^2$. [b] Weighting scheme: $w = 4(F_o)^2[\sigma^2/(F_o)^2]^2$. [c] All calculations were performed by using the TEXSAN-TEXRAY Structure Analysis Package, Molecular Structure Corp., 1985. Refinement was by full-matrix least-squares.

(24) Ying, W.-L.; Emerson, J.; Clarke, M. J.; Sanadi, D. R. *Biochemistry* **1991**, *30*, 4949–4952.
(25) Vasington, F. D.; Gazzotti, P.; Tiozzo, R.; Carafoli, E. *Biochim. Biophys. Acta.* **1972**, *256*, 43–54.
(26) Geselowitz, D.; Meyer, T. *Inorg. Chem.* **1990**, *29*, 3894–3896.
(27) Raven, S. J.; Meyer, T. J. *Inorg. Chem.* **1988**, *27*, 4478–4483.
(28) Yao, G. J.; Kira, A.; Kaneko, M. *J. Chem. Soc., Faraday Trans. 1* **1988**, *84*, 4451–4456.
(29) Clarke, M. J.; Jansen, B.; Marx, K. A.; Kruger, R. *Inorg. Chim. Acta* **1986**, *124*, 13–28.
(30) O'Connor, C. J. *Prog. Inorg. Chem.* **1982**, *29*, 203–285.

Table II. Atomic Positions in μ-O-[$(HCO_2)(NH_3)_4Ru]_2Cl_3$

atom	x	y	z	B^a
Ru	0.59689(3)	0.12163(2)	0.2075	1.10(1)
Cl(1)	1/2	0	0.708(1)	2.24(5)
Cl(2)	0.1044(1)	0.1520(1)	0.2063(9)	2.75(5)
O(1)	1/2	0	0.216(2)	1.4(1)
O(2)	0.6993(3)	0.2591(2)	0.207(2)	2.1(1)
O(3)	0.4845(4)	0.3562(3)	0.214(2)	3.0(2)
N(1)	0.451(1)	0.1727(6)	0.005(1)	2.2(3)
N(2)	0.767(1)	0.0717(7)	0.022(1)	2.3(3)
N(3)	0.7572(9)	0.0800(7)	0.402(1)	2.1(3)
N(4)	0.4448(9)	0.1732(5)	0.402(1)	1.3(3)
C(1)	0.6244(6)	0.3434(4)	0.204(3)	2.5(2)

$^a B_{eq} = \frac{8\pi^2}{3}\sum_{i=1}^{3}\sum_{j=1}^{3} U_{ij} a_i^* a_j^* \mathbf{a}_i \mathbf{a}_j$.

are listed in Table II. The intensities of three representative reflections, which were measured after every 150 reflections, remained constant throughout data collection, so that no decay correction was necessary. An empirical absorption correction, based on azimuthal scans of several reflections, was applied. The Ru atom was located by direct methods and the structure solved from difference Fourier maps. The non-hydrogen atoms were refined anisotropically. Hydrogen atoms were included in the structure factor calculation in idealized positions (C–H = 0.95 Å, N–H = 0.87 Å) and were assigned isotropic thermal parameters, which were 20% greater than the B_{equiv} value of the atom to which they were bonded. Refinement was by full-matrix least-squares. Neutral atom scattering factors[31] and anomalous dispersion effects were included in F_{calc};[32] the values for $\Delta f'$ and $\Delta f''$ were those of Cromer.[33]

Kinetics. The aquation of both the chloride- and formate-capped complexes was followed at 360 nm at 24 °C and μ = 0.1 adjusted with $NaClO_4$. Stock solutions of the μ-oxo compounds were prepared in distilled water. Buffering in the neutral pH range (5.0–8.0) was provided by 0.02 M phosphate (NaH_2PO_4/Na_2HPO_4) buffer. At low pH, solutions of perchloric acid (0.01–0.75 M) were used. Reactant solutions were obtained by mixing stock solutions of either the chloride (21.5 μM) or formate complexes (23.5 μM) with the same volume of buffer or acid of twice the desired final concentration. Reactions were allowed to run for approximately ten half-lives before measuring A_∞.

The decomposition of μ-O-$[(HO)(NH_3)_4Ru]^{3+}{}_2$ was monitored spectrophotometrically at 360 nm with an isosbestic point observed at 323 nm. Reactions were run in 0.1 M $NaClO_4$ with pH maintained by 0.02 M phosphate adjusted with 0.1 M NaOH. For all reactions, observed rate constants were determined from the least-squares slope of plots of $\ln(A - A_\infty)$ versus time. Fits of plots of k_{obs} versus pH were carried out by standard nonlinear regression techniques.

MO and MM Energy Calculations. ZINDO (INDO/1),[34] IEHT,[35] and molecular mechanics (MM2)[36] calculations were performed on a CaChe workstation[37] by using the crystallographic coordinates in Table II or idealized structures with octahedral geometry around the Ru atoms (Ru–N, 2.11 Å) and Cl's in the apical positions (Ru–Cl, 2.24 Å).

Results

Synthesis and Characterization. Separation of a commercial preparation of ruthenium red (Johnson-Matthey) on a Whatman CM-52 column eluted with 0.4 M ammonium formate yielded 13% (by weight) of the dimeric material absorbing at 360 nm. Consistent with its tripositive versus the hexapositive charge for ruthenium red, the dimeric formato-capped complex eluted from both Whatman CM-52 and Sephadex SP-25 ion exchange resins with 0.4 M ammonium formate as opposed to >0.6 M for ruthenium red, and the chloro-capped complex eluted from Dowex-50 with 3 M HCl. When the chloride capped complex was exchanged back to formate by elution from a BioRex 70 column, 1.2–1.4 M ammonium formate was used. Allowing chromatographically purified samples of the formato complex to remain on a column for extended lengths of time at neutral pH resulted in increasing amounts of a brownish-red irreversibly adhered material. Allowing either complex to reside for long periods of time on carboxylate ion-exchange columns led to strong binding to the column.

Table III. UV–Vis–Near-IR Spectral and Electrochemical Data for μ-O-$[L(NH_3)_4Ru]_2{}^{2+}$

ligand	λ (nm)	ε (M^{-1} cm^{-1})
HCO_2^-	360	2.1×10^4
	614	141
	1180	99
Cl^-	353	7.6×10^3
	614	149
	1107	390
H_2O (pH 2–3.4)	335	1.3×10^4
	593	121
	1185	324
OH^- (pH 9)	360	2.01×10^4
	612	153

Solutions and crystals of μ-O-$[(HCO_2)(NH_3)_4Ru]_2Cl_3$ generally appeared red in transmitted light and green in reflected light. Its UV–visible spectrum and that for the chloro complex are summarized in Table III. Plots of absorbance versus pH from spectrophotometric titrations of μ-O-$[(H_2O)_2(NH_3)_4Ru]_2{}^{5+}$ yielded $pK_{a1} = 4.18 \pm 0.08$ and $pK_{a2} = 7.2 \pm 0.1$, corresponding to individual proton ionizations from the coordinated waters to yield $[(HO)_2(NH_3)_4Ru]_2{}^{3+}$ above neutral pH. In agreement with this, titrations of μ-O-$[(H_2O)_2(NH_3)_4Ru]_2(ClO_4)_5 \cdot 2H_2O$ in water with NaOH indicated 1.95 ± 0.04 protons to be ionized between pH 3 and 10 with single-proton buffer regions corresponding to the spectrophotometrically measured pK_a's. Spectrophotometric observation of the second pK_a is somewhat obscured by the decomposition of the complex at high pH (see below).

Electrochemistry. Cyclic and square-wave voltammetric scans of μ-O-$[(HCO_2)(NH_3)_4Ru]_2{}^{3+}$ shown in Figure 1 reveal two reversible waves on relatively rapid scans between –0.3 and 1.2 V. When the negative switching potential was lower than –0.4 V, a third, broad, irreversible peak is evident around –0.3 V. At a scan rate of 150–300 mV/s, the couple at –4 mV becomes irreversible, as judged by the lower oxidation current in the cyclic voltammetric waveform. The three waves are assigned as Ru^{IV}–O–$Ru^{IV} \rightarrow Ru^{IV}$–O–$Ru^{III} \rightarrow Ru^{III}$–O–$Ru^{III}$ (E_2); Ru^{III}–O–$Ru^{III} \rightarrow Ru^{III}$–O–$Ru^{II}$ (E_3). The reduction potentials for both complexes are summarized in Table IV. In perchlorate media (μ = 0.1), the couples corresponding to E_2 and E_3 for μ-O-$[(HO)(NH_3)_4Ru]^{3+}{}_2$ appeared reversible above pH 4.1. The couple for E_4 (Ru^{III}–O–$Ru^{II} \rightarrow Ru^{II}$–O–$Ru^{II}$) is irreversible at all pH's values and merges with E_3 around pH 4–5.

Structure. The structure of μ-O-$[(HCO_2)(NH_3)_4Ru]^{3+}{}_2$ shown in Figure 2 reveals the complex ion to be a nearly linear dimer containing two octahedral rutheniums linked by an oxygen bridge with the ends of the molecule capped with formates. Selected bond distances and angles are listed in Tables V and VI, respectively. The bridging Ru–O bond is quite short, while the $Ru–O_{formate}$ bond length is typical for a Ru–O single bond.[38] The equatorial ammine–ruthenium bond lengths, which average 2.11(2) Å, are well within the expected range for a Ru–N single-bond distance. The Ru–Ru internuclear distance is 3.6463(6) Å. The two halves of the molecule are identical in that they are related by a C_2 axis along c. This passes through the bridging oxygen, is contained in a plane essentially perpendicular to that defined

(31) Cromer, D. T.; Weber, J. T. *International Tables for X-ray Crystallography*; Kynoch Press: Birmingham, England, 1974; Vol. IV, Tables 2.2A and 2.3.1.
(32) Ibers, J. A.; Hamilton, W. C. *Acta Crystallogr.* **1964**, *17*, 781–782.
(33) TEXSAN-TEXRAY Structure Analysis Package, 1985, Molecular Structure Corp., The Woodlands, TX 77381.
(34) Anderson, W. P.; Cundarai, T. R.; Drago, R. S.; Zerner, M. C. *Inorg. Chem.* **1990**, *29*, 1–3.
(35) Hoffmann, R. *J. Chem. Phys.* **1963**, *39*, 1397–1412.
(36) Allinger, N. L. *J. Am. Chem. Soc.* **1977**, *99*, 8127.
(37) CAChe, ZINDO, 2.8, 1991, Terra Pacific Writing Corp., Beaverton, OR 97075.
(38) Orpen, A. G.; Brammer, L.; Allen, F. H.; Kennard, O.; Watson, D. G.; Taylor, R. *J. Chem. Soc., Dalton Trans.* **1989**, S1-SS83.

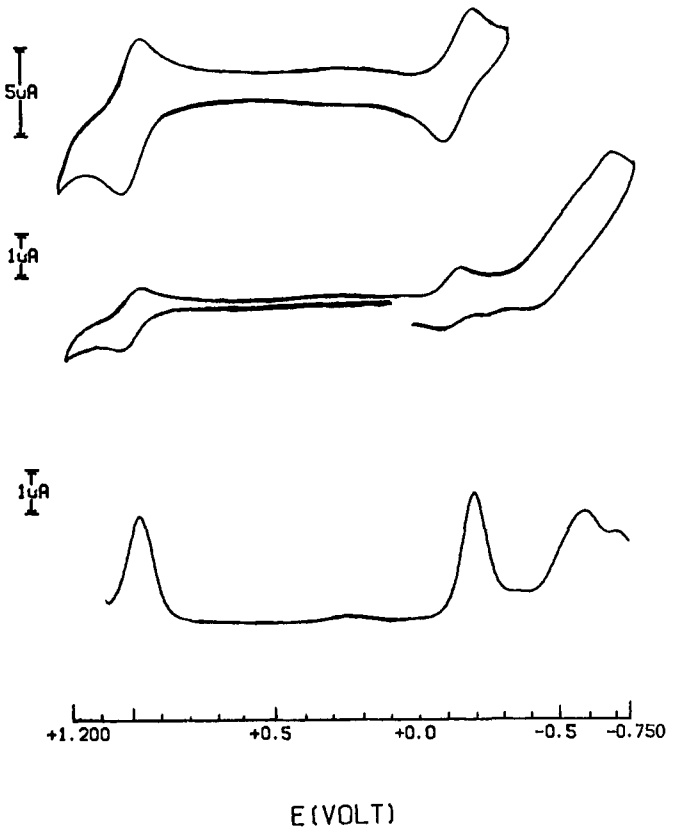

Figure 1. Top: cyclic voltammetric scan of μ-O-[$(HCO_2)(NH_3)_4Ru]_2^{3+}$ in 0.1 M LiCl at pH 3.6, switching potential –0.4 V. Middle: same, but with switching potential at –0.75 V. Bottom, square-wave voltammetry over same region. Electrodes: Ag/AgCl, reference; Pt wire, auxiliary; carbon paste, working. Scan rates: 500 mV/s, cyclic; 60 mV/s, square-wave.

Table IV. Electrochemical Data for μ-O-[$L(NH_3)_4Ru]_2^{2+}$

	reduction potential (V)			
L	$E°_1$ [IV–IV]/ [III–IV]	$E°_2$ [III–IV]/ [III–III]	$E°_3$ [III–III]/ [II–III]	$E°_4$ [II–III]/ [II–II]
HCO_2^-	1.173	0.004	~–0.40 (irrev)	
Cl^-	1.032	0.179	~–0.18 (irrev)	
H_2O (pH 2)		~0.7 (irrev)	0.18	~–0.04 (irrev)
OH^- (pH 8)		0.24	~–0.34	~–0.52 (irrev)
NH_3 (in CH_3CN)	1.91	0.56	–1.74	

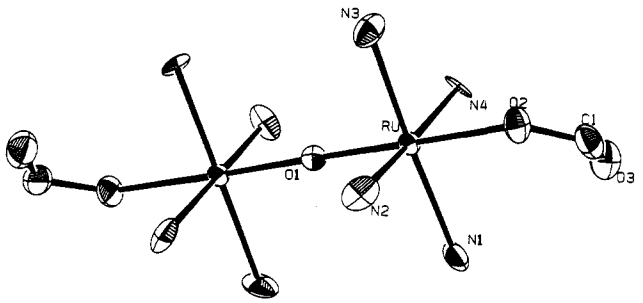

Figure 2. ORTEP[53] diagram of μ-O-[$(HCO_2)(NH_3)_4Ru]_2^{3+}$.

by the formates, and bisects the N1–Ru–N2 angle. (The formate plane is canted at a 42° angle with respect to the plane defined by N2, N4, O1, and O2). The four ammines around each Ru are nearly eclipsed with respect to one another with dihedral angles of 3.7°. The Ru is displaced out of the plane defined by the four ammines by 0.063 Å toward the bridging oxygen. The N1–O3 and N4–O3 distances of 2.93(1) and 2.85(1) Å, respectively, indicate intramolecular hydrogen bonding between these ammines and the pendant formate oxygen.[39] O3 is also intermolecularly hydrogen bonded to N2 and N3 of a symmetry-related molecule at distances of 3.14(2) and 3.19(2) Å, respectively. Cl1 is extensively hydrogen bonded to all nitrogens at distances of 3.248–3.384 Å as is Cl2 at distances between 3.293 and 3.477 Å.

Table V. Selected Bond Distances in μ-O-[$(HCO_2)(NH_3)_4Ru]_2Cl_3$

atom 1	atom 2	bond distance (Å)
Ru	O(1)	1.8240(6)
Ru	O(2)	2.033(3)
Ru	N(1)	2.101(9)
Ru	N(2)	2.139(9)
Ru	N(3)	2.094(9)
Ru	N(4)	2.091(8)
O(2)	C(1)	1.295(6)
O(3)	C(1)	1.217(6)

Table VI. Bond Angles Surrounding the Ru Atom and in μ-O-[$(HCO_2)(NH_3)_4Ru]_2Cl_3$

atom 1	atom 2	atom 3	angle (deg)
Ru	O(1)	Ru	176(1)
Ru	O(2)	C(1)	124.6(3)
O(1)	Ru	O(2)	177.7(5)
O(1)	Ru	N(1)	92.3(4)
O(1)	Ru	N(2)	93.2(4)
O(1)	Ru	N(3)	92.3(4)
O(1)	Ru	N(4)	89.1(4)
O(2)	Ru	N(1)	87.9(4)
O(2)	Ru	N(2)	89.0(4)
O(2)	Ru	N(3)	87.5(4)
O(2)	Ru	N(4)	88.6(3)
N(1)	Ru	N(2)	91.3(4)
N(1)	Ru	N(3)	174.8(3)
N(1)	Ru	N(4)	92.4(2)
N(2)	Ru	N(3)	86.2(2)
N(2)	Ru	N(4)	175.6(3)
N(3)	Ru	N(4)	89.9(3)

Aquation and Decomposition Rates. While the aquation of μ-O-[$(HCO_2)(NH_3)_4Ru]^{3+}{}_2$ almost certainly proceeds by a stepwise path in which first one and then the other formate ligand is lost, evidence for this was not observed in the plots of absorbance versus time. Consequently, the data was treated as single-step process which was first order in the ruthenium complex. The variation in the observed rate constant as a function of pH is illustrated in Figure 3A and is expressed as

$$k_{obs} = \frac{k_1[H^+]^2 + k_2[H^+]K_{a1} + k_3K_{a1}K_{a2}}{[H^+]^2 + [H^+]K_a + K_{a1}K_{a2}}\ s^{-1}$$

where $k_1 = (7.8 \pm 0.1) \times 10^{-3}\ s^{-1}$, $k_2 = (1.2 \pm 0.1) \times 10^{-4}\ s^{-1}$, $k_3 = \sim 4 \times 10^{-4}\ s^{-1}$, $pK_{a1} = 2.45 \pm 0.07$, and $pK_{a2} = \sim 9$. The analogous plot for the chloro complex is shown in Figure 3B, where $k_1 = (7.7 \pm 0.2) \times 10^{-3}\ s^{-1}$, $k_2 = (3.5 \pm 0.1) \times 10^{-4}\ s^{-1}$, $k_3 = 0.12 \pm 0.1\ s^{-1}$, $pK_{a1} = 2.03 \pm 0.09$, and $pK_{a2} = \sim 10.2$.

The aqua complex was observed to undergo an irreversible transformation above pH 7 with the observed rate law

$$\text{rate} = k_{obs}[Ru]$$

where

$$k_{obs} = \frac{k_1[H^+]K_{a1} + k_2K_{a1}K_{a2}}{[H^+]^2 + [H^+]K_a + K_{a1}K_{a2}}\ s^{-1}$$

and $k_1 = (6.8 \pm 0.7) \times 10^{-4}\ s^{-1}$, $k_2 = (2.3 \pm 1) \times 10^{-3}\ s^{-1}$, $pK_{a1} = 9.7 \pm 0.1$, and $pK_{a2} = 12.3 \pm 0.4$. The rate was independent of $[O_2]$. Solutions of μ-O-[$(HO)_2(NH_3)_4Ru]_2^{3+}$ which were allowed to stand in solution eventually yielded a dark precipitate.

(39) Huheey, J. E. *Principles of Inorganic Chemistry*; Harper & Row: New York, 1983; p 268.

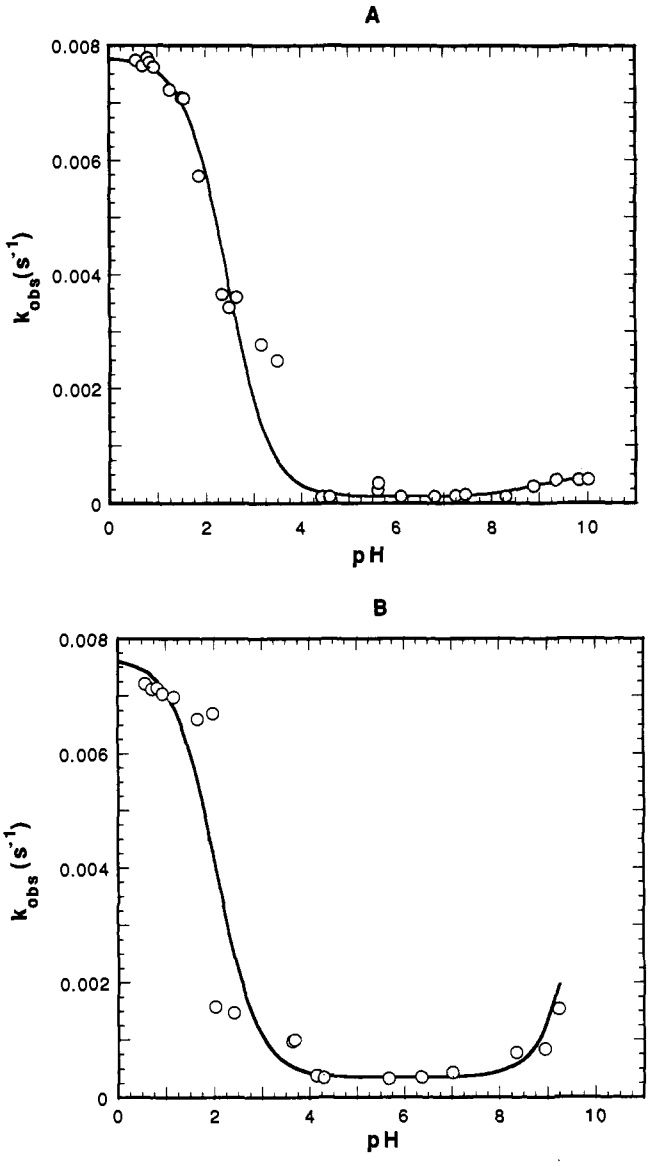

Figure 3. (A) Plot of k_{obs} for the aquation of μ-O-$[(HCO_2)(NH_3)_4Ru]_2^{3+}$ as a function of pH in $NaClO_4$, μ = 1.0. (B) Same for μ-O-$[Cl(NH_3)_4Ru]_2^{3+}$.

Chromatography of these solutions yielded a dark, immobile band at the top of an ion-exchange column.

MO and MM Energy Calculations. Both MM2 and INDO/1 calculations indicated no difference in energy with the tetraammine groups in either the staggered or eclipsed positions at a Ru–O–Ru bond angle of 180°. MM2 calculations revealed only small barriers to rotation of the tetraammine groups relative to one another at Ru–O–Ru bond angles between 155° and 180°. At 155°, the rotational barrier was <2 kcal/mol. INDO/1 calculations showed no activation barrier to bending of the Ru–O–Ru bond between 155° and 180° and yielded a parabolic fit parameter of 0.14 ± 0.01 kcal/deg^2 at bond angles less than 155°. MM2 calculations yielded a parabolic fit parameter of only 8.4×10^{-2} kcal/deg^2 at bond angles >155° but significantly higher values for more acute angles. The Wyberg bond indices for Ru–O (0.83, INDO; 1.09, IEHT) are significantly greater than those for Ru–N (0.74, INDO; 0.59, IEHT). IEHT calculations on idealized structures with Ru–O–Ru angles of both 150° and 180° showed the charge to be evenly distributed between the two ruthenium centers and there to be a substantial bonding interaction between them. Similar results were obtained from INDO/1 calculations on the same structures, except that the Wyberg bond index between the two rutheniums was much lower. When the geometry was optimized by INDO/1 calculations with

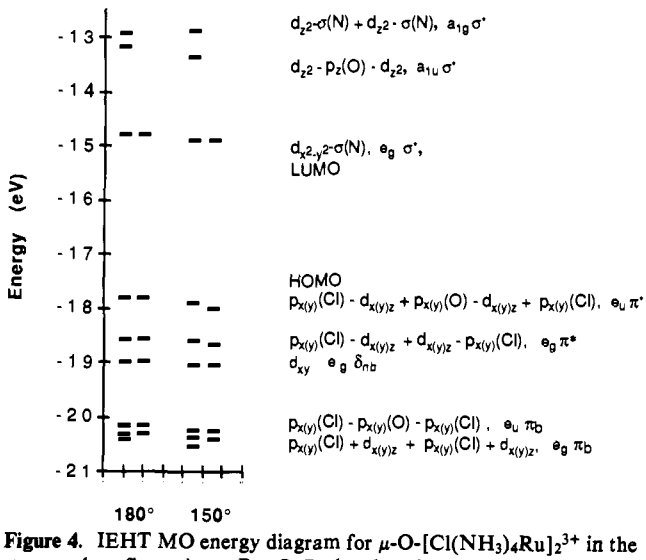

Figure 4. IEHT MO energy diagram for μ-O-$[Cl(NH_3)_4Ru]_2^{3+}$ in the staggered configuration at Ru–O–Ru bond angles of 180° and 150° with all other bond lengths idealized as the average of the crystallographic distances and octahedral geometry around each Ru. Symmetry designations are given in D_{4h}.

no constraints, the formal charge on the two metal ions differed by only 0.02 with the INDO Wyberg Ru–Ru bond index remaining about the same. The molecular orbital energy levels as calculated by IEHT methods are shown in Figure 4.

Discussion

Structure. The μ-O–Ru bond length is slightly shorter than those found in ruthenium red (1.84–1.86 Å)[22] and in a related complex in which the central ruthenium's ammine ligands are substituted with ethylenediamines (1.85–1.89 Å).[40] In these trimers, the Ru–μ-O bonds are probably slightly lengthened by mutual *trans* influences generated by the μ-oxo groups. The short μ-oxo bonds in all of these structures indicate significant π-bonding involving p-orbitals on the oxygen and d_π orbitals on the metal ions, which have lobes of π-symmetry directed down the internuclear z-axis.[41] In the present complex, since the odd anionic charge of 7 must be balanced by that of two symmetry related ruthenium ions, the metal ions should be considered as Ru(3.5) with the odd electron delocalized through the π-bonding network between the two metals.

While the arrangement of the two quartets of equatorial ammines on each ruthenium into a nearly eclipsed conformation suggests that there may be some direct δ-bonding between the two ruthenium ions mediated by their d_π-orbitals, the long internuclear distance of greater than 3.6 Å minimizes this possibility and indicates that the eclipsed conformation is due to packing forces. An analogous arrangement appears in the crystal structure of ruthenium red,[22] in which the middle ensemble of equatorial ammines is eclipsed with one end set and staggered with the other, while in the related ethylenediamine structure both end sets of ammines are staggered relative to ethylenediamine nitrogens on the middle ruthenium.[40] In harmony with an earlier indication that the barrier to bending along the Ru–O–Ru axis is small,[42] INDO/1 calculations revealed no significant activation energy to bending between 155° and 180°. Indeed, while μ-O-$[Cl_5Ru]^{4-}{}_2$ and the ethylenediamine derivative of ruthenium red are nearly linear, μ-O-$[NO_2(bpy)_2Ru]_2$ is bent to an angle of 157.2°, and ruthenium red is linear between Ru(2) and Ru(3) but bent (171°) between Ru(1) and Ru(2). Figure 4 shows that most HOMO levels become slightly more stable on bending. This

(40) Smith, P. M.; Fealey, T.; Earley, J. E.; Silverton, J. V. *Inorg. Chem.* **1971**, *10*, 1943–1947.
(41) Dunitz, J. D.; Orgel, L. E. *J. Chem. Soc.* **1953**, 2594–2596.
(42) Burchfield, D. E.; Richman, R. M. *Inorg. Chem.* **1985**, *24*, 852–857.

is due to both a change in oxygen hybridization and a "Jahn–Teller" effect breaking the degeneracy of the half-occupied HOMO. On the other hand, these stabilization processes are approximately evenly balanced by increasing steric repulsion between the tetraammine groups. Consequently, the low or absent activation barriers to both bending and rotation about the Ru–O–Ru axis make these ions highly deformable.

The capping formate ions evident in Figure 2 were added onto the ion during the chromatographic purification. Similarly, the formates can be replaced by chlorides on cation-exchange chromatographic columns eluted with HCl followed by warming in constant boiling HCl on removing the eluant by rotary evaporation. This implies that the end positions of the dimeric core can be substituted by high concentrations of good ligands and may be somewhat labilized by the bridging oxygen. Consequently, while solutions of the characterized complex inhibit calcium ion uptake in mitochondria,[24] the active component in ruthenium red is very likely $[X(NH_3)_4Ru–O–Ru(NH_3)_4X]^{3+}$, where X = Cl^- or OH^-. Since the chloride-capped complex had a much higher affinity for the carboxylate cation-exchange column than the formate-capped ion, it is likely that some degree of covalent binding occurred via substitution of the chloride by carboxylates on the column.

Spectra and Electrochemistry. The reduction potentials of the complexes are such that they are mixed-valent in aerobic aqueous solutions. The cyclic voltammetric data indicate that the [3.5–3.5] complex can be reversibly reduced to the [III–III] and [II–III] states, at least on a rapid time scale. Further reduction appears to lead to decomposition. This probably arises from dissociation of the complex because Ru^{II} cannot π-bond to the bridging oxygen, which is probably protonated to water. The large comproportionation constants for the formato and chloro complexes (K_{com} = 5.7 × 10^{19} and 2.9 × 10^{14}, respectively) calculated from E_1 and E_2 are consistent with strong electronic coupling leading to two equivalent metal centers. All of this is in concert with the nature of the HOMOs as calculated by IEHT or INDO/1 as being delocalized π^*.

Owing to its higher charge, the E_2 value for μ-O-$[(H_2O)_2(NH_3)_4Ru]_2^{5+}$ is substantially higher than those of the chloro and formato complexes. Similarly, its E_1 potential occurs above that for water oxidation and cannot be observed. The pK_a value for $[(H_2O)(NH_3)_5Ru]^{3+}$ is 4.1, while that for $[(H_2O)(bpy)(py)Ru]^{3+}$ is 0.85.[43] Among similar μ-oxo complexes, the pK_a for $[(H_2O)(bpy)_2Ru^{III}ORu^{IV}(bpy)_2(OH_2)]^{5+}$ is 0.4, while that for $[(H_2O)(bpy)_2Ru^{III}ORu^{IV}(bpy)_2(OH)]^{4+}$ is 3.3.[44] Since ammonia is a better σ-donor than bipyridine and some additional electron density might be expected for the position *trans* to the μ-oxo, the pK_a values reported here for $[(H_2O)(NH_3)_4RuORu(NH_3)_4(OH_2)]^{5+}$ and $[(H_2O)(NH_3)_4RuORu(NH_3)_4(OH)]^{4+}$ are reasonable. The pH titrations indicate that each of the two inflections evident in the spectrophotometric titration consists of overlapping single-proton ionizations. Consequently, these are assigned as

$$[(H_2O)(NH_3)_4RuORu(NH_3)_4(OH_2)]^{5+} \xrightarrow{K_{ox1}} [(H_2O)(NH_3)_4RuORu(NH_3)_4(OH)]^{4+} \xrightarrow{K_{ox2}} [(HO)(NH_3)_4RuORu(NH_3)_4(OH)]^{3+}$$

The 2.0 unit separation of the pK_a values is significantly greater than the statistical factor of 0.301, which is consistent with the two metal centers being in close electronic communication. The pH behavior of the redox couples is complicated by the irreversibility of E_2 at low pH and the merging of E_3 and E_4 at $4 < pH < 5$. It is also likely that, in addition to proton equilibria involving the apical H_2O/OH^- ligands, the bridging ligand is protonated in the reduced forms. While there is little data on ionization constants for bridging oxides, the μ-O in an oxo-bridged $\{Mn^{IV}_4O_6\}^{4+}$ cluster exhibits a pK_a ~3.5.[45]

The [IV–III] complex can be expected to be analogous to $[(NH_3)_5Ru–O–Ru(NH_3)_5]^{5+}$,[46] which has a similar absorption spectrum in that it exhibits an intense absorption at 342 nm (ϵ = 2.53 × 10^4 M^{-1} cm^{-1}) and a weak one at 616 nm (ϵ = 251 M^{-1} cm^{-1}) (C_{2v}, near-IR not reported).[41,42,46] In D_{4h} symmetry, the metal d_{xz} and d_{yz} orbitals mix with the μ-oxo p_x and p_y to form an $e_u(\pi)$ and $e_u^*(\pi^*)$ set. Since the spectra reported here are relatively independent of the apical ligands and are similar to those reported for μ-O-$[(NH_3)_5Ru]_2^{5+}$,[42,46] it may be reasonably assumed that the bands involve transitions between MOs involving mainly O and Ru. With this in mind, there is good agreement between the three observed transitions and the energies of these transitions calculated by IEHT; however, these differ from previously reported assignments made on qualitative symmetry arguments.[46] For μ-O-$[Cl(NH_3)_4Ru]_2^{5+}$ the assignments with observed and calculated λ_{max} (Ru–O–Ru bond angle = 180°, D_{4h}) are d_{xy} (e_g, nb) → $p_{x(y)}(Cl) - d_{x(y)z} + p_{x(y)}(O) - d_{x(y)z} + p_{x(y)}(Cl)$ (e_u, π^*) at 1077 (1107) nm; $p_{x(y)}(Cl) - p_{x(y)}(O) - p_{x(y)}(Cl)$ (e_u π_b) → $p_{x(y)}(Cl) - d_{x(y)z} + p_{x(y)}(O) - d_{x(y)z} + p_{x(y)}(Cl)$ ($e_u\pi^*$) at 614 (532) nm; and $p_{x(y)}(Cl) - d_{x(y)z} + p_{x(y)}(O) - d_{x(y)z} + p_{x(y)}(Cl)$ ($e_u\pi^*$) → $d_{x^2-y^2} - \sigma(N)$ ($e_g\sigma^*$) at 353 (409) nm. In keeping with its low intensity, the transition at 614 nm is symmetry disallowed in D_{4h} symmetry. On the other hand, the intense transition, which gives the complex its color, is largely charge transfer in character. It should be noted that IEHT calculations do not take spin energies into account and *ab initio* calculations by Ondrochen suggest that the 1077 and 614 nm transitions may arise from the $e_u(\pi^*)$ and $e_g(\pi^*)$ levels, respectively.[47] Owing to the small bending energy, substantial broadening in these bands is expected as the nondegeneracy of the orbitals is lifted on decreasing the Ru–O–Ru angle to 150°. Similar to ruthenium red, whose intense color also derives from a transition between similar sets of orbitals,[48] these complexes exhibit the peculiar optical property of appearing red or green as a function of the angle of the incident light.

Consistent with little participation from the apical ligands in the HOMO, the reduction potentials of μ-oxo ruthenium dinuclear complexes are only slightly dependent on ligands with the same charge (cf. Table IV). Since $[(NH_3)_5Ru–O–Ru(NH_3)_5]^{5+}$ is reversibly reduced to the [III–III] state at 0.56 V (vs SHE) in acetonitrile, it is reasonable that the analogous reduction for μ-O-$[(HCO_2)(NH_3)_4Ru]^{3+}_2$ is also reversible, while the lower reduction potential for the latter ion can be attributed to the presence of the anionic formates. Another difference is that the oxidation of μ-O-$[(NH_3)_5Ru]^{5+}_2$ to the [IV–IV] state is irreversible while that for μ-O-$[(HCO_2)(NH_3)_4Ru]^{3+}_2$ is reversible, which may also be attributed to the presence of the formates stabilizing the higher oxidation state by charge donation to the d_π-orbitals of the rutheniums. On the other hand, the more highly charged aqua complex is better able to tolerate reduction to μ-O-$[(H_2O)(NH_3)_4Ru]^{3+}_2$, at least on the electrochemical time scale.

Magnetism. The magnetic properties of Ru^{III} in axial environments are strongly dependent on the spin-orbit coupling constant (ζ) and the axial crystal field splitting parameter (Δ)[49] and are somewhat less dependent on the orbital overlap reduction factor (k).[50] Spin–orbit coupling also relaxes the electronic spin such that ESR signals are often severely broadened. Consequently, the broad somewhat featureless ESR signal observed in frozen solution is not unusual. Similarly, L–S coupling can also

(43) Moyer, B. A.; Meyer, T. J. *Inorg. Chem.* **1981**, *20*, 436–444.
(44) Doppelt, P.; Meyer, T. J. *Inorg. Chem.* **1987**, *26*, 2027–2034.
(45) Hagen, K. S.; Westmoreland, T. D.; Scott, M. J.; Armstrong, W. H. *J. Am. Chem. Soc.* **1989**, *111*, 1907–1909.
(46) Baumann, J. A.; Meyer, T. J. *Inorg. Chem.* **1980**, *19*, 345–350.
(47) Wu, M. Ph.D. Thesis, Northeastern University, 1993.
(48) Earley, J. E.; Fealey, T. *Inorg. Chem.* **1973**, *12*, 323–327.
(49) Carlin, R. L. *Magnetochemistry*; Springer-Verlag: New York, 1986.
(50) Stevens, K. W. H. *Proc. R. Soc. London, A* **1953**, *219*, 542–555.

account for μ_{eff} values above 2.5.[51] Since both IEHT and Hartree–Fock–Slater/SCF[47] calculations suggest excited states with higher spin lying only slightly above the $S = {}^1/_2$ ground state, interactions involving these states, some of which may be thought of as involving two spin systems of $S = {}^1/_2$ (Ru^{III}) and $S = 1$ (Ru^{IV}),[30] may also play a role in the observed μ_{eff}.

Aquation and Decomposition Rates. The variation in the observed rate constant for the aquation of both μ-O-[$(HCO_2)(NH_3)_4Ru]^{3+}{}_2$ and the analogous chloro complex as a function of pH (see Figure 4) indicates that the parent complex is activated toward aquation by both protonation and deprotonation. While protonation would seem more likely on the formato carbonyl, the similarity in parts A and B of Figure 3 suggests common ionization sites, which may involve protonation of the μ-O at low pH and ionization of a *cis*-ammine at high pH. Indeed, both the aquation and decomposition reactions are consistent with an ionization process above pH 9–10, which is in the range expected for an ammine hydrogen on Ru(3.5).[52,53]

Conclusion. The complex $[Cl(NH_3)_4Ru–O–Ru(NH_3)_4Cl]^{3+}$ constitutes a significant portion of the "ruthenium red" cytological stain,[24] and the hydroxy analog readily forms in water. Their tripositive charge, hydrogen bonding capability, and ability to readily deform should allow them to bind to a variety of anionic carboxylate sites on proteins including Ca^{2+} receptors. Decomposition of the hydroxo-capped complex at physiological pH also yields a substance that irreversibly binds to polyanionic materials. Their smaller size and ability to covalently bind to amino acid functional groups at their apical sites may account for their greater biochemical activity relative to ruthenium red. By competing for the same sorts of binding sites as ruthenium red, the dimeric complexes with their relatively low visible absorption can be expected to interfere with visual staining. On the other hand, it is likely that they are also responsible for at least a portion of "ruthenium red's" ability to stain for electron microscopy. Binding through their apical sites may provide a means of covalently linking the $[Ru–O–Ru]^{5+}$ core to chromatographic substrates in order to serve as an affinity agent for Ca^{2+} receptor proteins, and substitution of the formates by water may open the way to the oxidative formation of linear $[O{=}Ru{-}O{-}Ru{=}O]^{3+,4+}$ cores to complement existing *cis*-dioxo cores useful in catalysis.[44]

Acknowledgment. This research was supported by PHS Grant GM26390. We appreciate helpful conversations with Prof. M. J. Ondrochen and Ms. M. Wu of Northeastern University.

Supplementary Material Available: UV–visible and Near-IR spectra of μ-O-$[(HCO_2)(NH_3)_4Ru]_2Cl_3$ and complete tables of crystallographic data, positional parameters, thermal parameters, bond distances, bond angles, and least-square planes (9 pages); table of F_c and F_o for μ-O-$[(HCO_2)(NH_3)_4Ru]_2Cl_3$ (7 pages). This material is contained in many libraries on microfiche, immediately follows this article in the microfilm version of the journal, and can be ordered from the ACS; see any current masthead page for ordering information.

(51) Earnshaw, A. *Introduction to Magnetochemistry*; Academic Press: New York, 1968.
(52) Waysbort, D.; Evenor, M.; Navon, G. *Inorg. Chem.* **1975**, *14*, 514–519.
(53) Johnson, C. K. ORTEPII. Report ORNL-5138; Oak Ridge National Laboratory: Oak Ridge, TN, 1976.